MICHIGAN STATE UNIVERSITY

CYCLOTRON LABORATORY

THE MSU MINIBALL 4π FRAGMENT DETECTION ARRAY

R.T. de SOUZA, N. CARLIN, Y.D. KIM,
J. OTTARSON, L. PHAIR, D.R. BOWMAN,
C.K. GELBKE, W.G. GONG, W.G. LYNCH,
R.A. PELAK, T. PETERSON, G. POGGI,
M.B. TSANG, and H.M. XU

APRIL 1990

MSUCL-720

MSUCL-720
April, 1990

"The MSU Miniball 4π fragment detection array"

R.T. de Souza, N. Carlin,* Y.D. Kim, J. Ottarson, L. Phsir, D.R. Bowman, C.K. Gelbke, W.G. Gong, W.G. Lynch, R.A. Pelak,† T. Peterson,†† G. Poggi,# M.B. Tsang, and H.M. Xu

National Superconducting Cyclotron Laboratory

and Department of Physics and Astronomy

Michigan State University, East Lansing, MI 48824, USA

Abstract: A compact and highly granular charged particle detection array, covering 89% of 4π in solid angle, is described. In its present configuration, the array consists of 188 fast-plastic CsI(Tl) phosnich detectors arranged in 11 rings coaxial about the beam axis. Each phosnioh detector is comprised of a 40μm thick plastic scintillator foil and a 2 cm thick CsI(Tl) crystal selected for good scintillation uniformity. The detectors are reed out by photomultiplier tubes. Elemental identification up to Z≈18 and isotopic identification of H and He nuclei is achieved by exploiting pulse shape discrimination techniques.

* Present address: Instituto de Física, Universidade de São Paulo, C. Postal 20516, CEP 01498, São Paulo, Brazil

† Present address: Department of Physics, Cornell University, Ithaca, NY 14853, USA

†† Present address: Department of Physics, Gustafus Adolfus College, Saint Peter, MN 56082, USA

Permanent address: Dipartimento di Pisica dell' Università and INFN, Largo Enrico Fermi 2, 60125 Firenze, Italy

1. Introduction

Highly excited nuclear systems, formed in intermediate and high energy nuclear reactions, can decay by emitting a considerable number of complex fragments [1]. Such multi-fragment emission processes are of particular interest, since they might provide important information about the liquid-gas phase diagram of nuclear matter [2,3]. At sufficiently high excitation energies, the internal pressure in the nuclear medium could be large enough to cause an expansion. If, during this expansion phase, the reaction trajectory in the temperature-density plane passes through the spinodal line, the system could become mechanically unstable against the growth of and decay by a multifragment disintegration [4-9]. Experimental evidence concerning the existence and characterization of a multi-fragment decay mode is still rather limited. In order to study multiple emission of complex fragments with nearly 4π coverage, we have constructed a fragment detection array of high granularity and low detection thresholds. In its present configuration, the device covers the angular range of Θ_{lab}= 9°-160° with 188 phoswich detectors consisting of 40 µm thick plastic scintillator foils and 2 cm thick CsI(Tl) scintillators. Thresholds for particle identification range from E/A≈1.5 MeV for alpha particles to E/A≈3 MeV for Ca ions. Individual detectors can resolve elements from Z≈1-18, as well as isotopes of hydrogen and helium. Charged particle detector arrays based on similar techniques have been described in refs. [10,11].

In this paper, we give a detailed description of the device and its performance characteristics. The mechanical construction of the array is described in Sect. 2. In Sects. 3-6, the detector design, the photomultiplier gain monitoring system, quality tests of CsI(Tl) crystals, and the technique for the fabrication of uniform thin scintillator foils will be presented. The

data acquisition electronics and test results for particle identification will be detailed in Sects. 7 and 8. A brief summary will be given in Sect. 9.

2. Mechanical Construction of the Array

The Miniball phoswich detector array is designed to operate in a vacuum vessel. An artist's perspective of the three-dimensional geometrical assembly is shown in Fig. 1. The array consists of 11 independent rings coaxial about the beam axis. For ease of assembly, as well as servicing, the individual rings are mounted on separate base plates which slide on two precision rails. The rings and detector mounts are made of aluminum. Good thermal conductivity between detectors and the mounting structure allows the conduction of heat generated by the photomultiplier voltage divider network into the array superstructure. This heat is removed from the Miniball by cooling the base plates. By this means, constant operating temperature in vacuum is achieved after a brief equilibration time. The individual detector mounts are designed to allow the removal of any detector without interfering with the alignment of neighboring detectors. The entire assembly is placed on an adjustable mounting structure which allows for the alignment of the apparatus with respect to the beam axis.

Figure 2 shows a half-plane section of the array in the vertical plane which contains the beam axis. Individual rings are labelled by the ring numbers 1-11 which increase from forward to backward angles. For each ring, the number of detectors is given in parentheses. For a given ring, the detectors are identical in shape and have the same polar angle coordinates with respect to the beam axis; these angles are indicated in Fig. 2. Since the angular distributions of the emitted particles are strongly forward peaked, the solid angle subtended by forward detectors is smaller than for backward detectors.

Variations in solid angle were achieved largely by placing detectors at different distances from the target while keeping their size approximately constant. The front face geometries of the individual CsI(Tl) crystals are shown in Fig. 3. Different detector shapes are labelled by the respective ring numbers with the number of detectors per ring given in parentheses (see Fig. 2 for the definition of the ring numbers). The crystals are tapered such that front and back surfaces subtend the same solid angle with respect to the target location. In order to save cost of fabrication, the curved surfaces corresponding to constant polar angle were approximated by planar surfaces. The resulting loss in solid angle coverage is on the order of 2%, comparable in magnitude to the loss in solid angle coverage resulting from gaps between individual detectors (which must be provided to allow for mechanical tolerances and optical isolation between neighboring crystals).

An isometric drawing of the target insertion mechanism is shown in Fig. 4. The targets are mounted on frames made of flat shim stock of 0.2 mm thickness. Each target frame is attached to an insertion rod. The insertion rods are mounted on a tray which can be moved parallel to the beam axis. An electromagnetic clutch provides the coupling to the insertion and retraction drive once a target rod is located at the appropriate position. A third drive allows rotation of an inserted target about the axis of the insertion rod. This rotation of the target plane is useful for the determination of the shadowing a detector experiences when it is located in the plane of the target frame.

In its present configuration, the detector array covers a solid angle corresponding to about 89% of 4π. The loss in solid angle can be decomposed into the following contributions: (i) beam entrance and exit holes (4% of 4π); (ii) approximation of the curved surfaces corresponding to constant polar angle by

planar surfaces (2% of 4π); (iii) optical isolation of detectors and allowance for mechanical tolerances (4% of 4π); (iv) removal of one detector at $\theta=90^\circ$ to provide space for target insertion mechanism (1% of 4π).

3. Detector Design

All phoswich detectors of the array are composed of a thin (typical thickness: 4 mg/cm^2 or 40 μm) plastic scintillator foil, spun from Bicron BC-498X scintillator solution, and a 2 cm CsI(Tl) scintillator crystal. A schematic of the detector design is given in Fig. 5. In order to retain flexibility in the choice of scintillator foil thickness, the scintillator foil is placed on the front face of the CsI(Tl) crystal without bonding material. (Tests indicate that slightly improved resolution can be achieved when the two scintillators are coupled via a thin layer of optical cement, see Sect. 8 below.) The back face of the CsI(Tl) scintillator is glued with optical cement (Bicron BC600) to a flat light guide made of UVT plexiglas. This light guide is 12 mm thick and matches the geometrical shape of the back face of the CsI(Tl) crystal. This light guide is glued to a second cylindrical piece of UVT plexiglas (9.5 mm thick and 25 mm diameter) which, in turn, is glued to the front window of the photomultiplier tube (Burle Industries model C83062E). The photomultiplier tube and the cylindrical light guide are surrounded by a cylindrical μ-metal shield (not shown in the figure). Front and back faces of the CsI(Tl) crystals are polished; the tapered sides are sanded and wrapped with white teflon tape. The front face of the phoswich assembly is covered by an aluminized mylar foil (0.15 mg/cm^2 mylar and 0.02 mg/cm^2 aluminum).

The primary scintillation of the plastic scintillator used has its maximum intensity at 370 nm. In bulk material of the scintillator, the intensity maximum is shifted to 420 nm by the addition of a wavelength shifter. Our

scintillator foils are, however, too thin for an effective wavelength shift and maximum emission remains in the far blue region of the spectrum. The absorption of this light in CsI(Tl) places a constraint on the maximum useful thickness of the CsI(Tl) crystals. Additional absorption in the light guides can be minimized by using UVT plexiglas rather than standard plexiglas light guides. Such considerations become particularly important for phoswich detectors utilizing thin scintillator foils in efforts to reduce particle detection thresholds.

Figure 6 shows a photograph of the basic photomultiplier assembly used for all detectors. The phoswich and matching first light guide have not yet been attached. A precision machined aluminum ring is glued to the μ-metal shield surrounding the photomultiplier and the cylindrical light guide. This ring provides the alignment for a precision machined aluminum can which houses the voltage divider and which defines the detector alignment when bolted to the rings of the array support structure. In order to expose the voltage divider chain, this aluminum can has been removed and placed next to the photomultiplier. The active voltage divider chain is soldered to the flying leads of the phototube. To prevent destruction of the FETs by sparking during operation in poor vacuum, the entire divider chain, including the leads to the photomultiplier tube, is encapsulated in silicone rubber (Dow Chemical Sylgard 184). Vacuum accidents occurring with fully biased detectors do not lead to divider chain failures. In fact, the detectors can survive a full pumping cycle from atmospheric pressure to vacuum with bias applied to them.

The 10-stage Burle Industries model C83062E photomultiplier tube was chosen because of its good timing characteristics ($\tau_R \approx 2.3$ ns), its large

nominal gain ($\approx 10^7$), and its good linearity for fast signals. Since the apparatus is designed to operate in vacuum, active divider chains were chosen to minimize the generation of heat. A schematic of the active divider chain is given in Fig. 7. The final stages of the divider stage are of the "booster" type which provides improved linearity for high peak currents generated by large signals of the fast scintillator.

4. Light Pulsing System

Gain drifts of the photomultiplier tubes are monitored by a simple and compact light pulser system which operates in vacuum. In order to preserve the modularity of the device and avoid unnecessary removal of optical fibers during transport, each detector ring is provided with its own light pulser system. Figure 8 shows schematics of the mechanical assembly of the light pulser system and of the driving circuit for the light emitting diodes (LEDs) which is triggered by an external NIM logic signal. During experiments, the light pulser is triggered at a rate of about 1 Hz. Light is generated by simultaneously pulsing an array of eight LEDs (Hewlett Packard HLMP-3950) which generate light at wavelengths around 565 nm. The emitted light is diffused by reflection from an inclined teflon surface. Light fibers which only view scattered light transport the light to the individual photomultipliers.

Because of temperature fluctuations and aging effects, operation of light emitting diodes is not stable over long periods of time. Therefore, the intensity of each light pulse is monitored by two PIN diodes (Hamamatsu S1223) read out by standard solid state detector electronics. The ratio of the signals of the two PIN diodes can be used to monitor their stability. The ratio of pin diode and photomultiplier signals can then be used to monitor the gain of the individual photomultiplier tubes according to the relation:

$$Ch' = Ch \times (Pin1+Pin2)/2Pmt \ . \qquad (1)$$

Here, Ch denotes the ADC conversion measured for a given event, Ch' is the conversion corrected for gain shifts, and Pmt, Pin1, and Pin2, are the channel numbers for LED generated light pulses detected by the individual photomultiplier tube and the two PIN diodes, respectively. Better than 1% gain stabilization is achieved if the temperature of the CsI(Tl) crystals is kept constant. (Variations of the scintillation efficiency of CsI(Tl) caused by temperature fluctuations cannot be detected with the light pulser.) It was verified, however, that active cooling of the base plate ensures rapid achievement of a stable operating temperature for the Miniball.

Figure 9 illustrates the gain stabilization achieved with the light pulser system. The gain variations of a photomultiplier (enhanced by variations of the supply voltage) were directly measured by irradiating a CsI(Tl) crystal with α-particles emitted from a collimated ^{228}Th source and monitoring the peak location of the 8.785 MeV α-line; they are shown by the open points in the figure. The solid points in the figure show the peak positions obtained in the off-line analysis after correcting the gain variations according to information from obtained by the light pulser system. Gain stability to better than 1% was achieved.

5. Uniformity of Scintillation Efficiency of CsI(Tl)

Previous experience with CsI(Tl) crystals used for the detection of energetic particles had revealed difficulties with the production of scintillators with uniform scintillation response [12,13]. Therefore, considerable attention was paid to select CsI(Tl) crystals of uniform scintillation efficiency. In previous tests of large cylindrical CsI(Tl) crystals [12,13], non-uniformities

of the scintillation efficiency were detected by measuring the response to collimated γ-rays. Such measurements are relatively easy to perform since they can be done in air. However, they are less suitable for small volume crystals, since collimated γ-rays sample a relatively large volume of the crystal. Small scale fluctuations of the scintillation efficiency may stay undetected. In addition, measurements for small non-cylindrical crystals are less precise, since the shape of the Compton background depends on the position of the collimated γ-ray source. Such dependences lead to additional uncertainties in the extraction of the photopeak position.

It was determined, however, that nonuniformities of the scintillation efficiency can be detected very sensitively by scanning the CsI(Tl) crystals with a collimated α-source in vacuum. All crystals ordered from various manufacturers were rectangular in shape with dimensions of 2"X1.5"X1". They were polished at the front and back faces (with dimensions of 2"X1.5") and sanded at the sides. The back face was optically coupled to a clear acrylic light guide with the same dimensions as the crystal. This light guide, in turn, was optically connected to a photomultiplier tube of 1" diameter. The sides of the CsI(Tl) crystal and of the light guide were wrapped with white teflon tape. By covering the front face of the CsI(Tl) scintillator with an aluminized mylar foil, a uniform light collection efficiency was achieved. (Without a reflective entrance foil, the light collection efficiency decreased by about 5% from the center of the front face to its sides.) The front face of the crystal was scanned in vacuum and the peak location of the 8.785 MeV α-line from a collimated ^{228}Th α-source was monitored. In order to avoid edge effects, regions within about 2 mm of the side boundaries of the crystal were not scanned. Most test were performed with a simple multichannel analyzer equipped with a peak sensing ADC; in those instances the anode signal of the

photomultiplier was shaped and amplified with standard electronics, using integration and differentiation times of 1 μs.

Figure 10 shows the results of a scan for a crystal exhibiting a large gradient of the scintillation efficiency. The horizontal axis of the plot shows the location of the collimated α-source with respect to the center, along the short symmetry axis of the front face. Different surface treatments of the front face of the scintillator did not affect the measured variation of the scintillation efficiency. In order to demonstrate that such variations were related to the bulk material of the scintillator we exchanged the role of front and back faces of this scintillator and performed an equivalent scan of the parallel surface (i.e. the previous back face). The results of the two scans are compared by the solid and open points in Fig. 10. (The coordinate system was kept fixed with respect to the CsI(Tl) crystal.) Nearly identical variations of the scintillation efficiency are observed across the two parallel scintillator surfaces indicating that the measured large gradient of the scintillation efficiency persists through the bulk material of the sample.

The measurements shown in Fig. 11 were performed by integrating the anode current of the photomultiplier with a charge integrating ADC using time gates of Δt = 0.1-0.5 μs and Δt = 1.1-4.1 μs which select the fast and slow scintillation components of CsI(Tl). The fast component exhibits a larger variation of the scintillation efficiency than the slow component. Since the relative intensity of fast and slow scintillation components depends strongly on the Tl concentration [14,15], the observed variations of scintillation efficiency are most likely due to gradients in the Tl concentration.

Crystals incorporated into the Miniball were preselected by scanning the 1.5"x2.0" rectangular surface of original crystals along two perpendicular axes and requiring a uniformity of scintillation response better than 3%. The preselected crystals were then milled into their final shapes and scanned a second time, requiring uniformity of response within 2.5%. The preselection process avoided expensive machining of poor quality crystals; it was about 90% efficient for the selection of crystals of the desired quality.

Figure 12 compares variations of scintillation efficiency detected with collimated α-particles of 8.785 MeV energy (source: ^{228}Th) and γ-rays of 662 keV energy (source: ^{137}Cs). The left and right hand panels give examples for a rejected and an accepted crystal, respectively. The enhanced sensitivity of the α-particle scan is obvious. It is probably caused by the fact that α-particles sample a much smaller volume than γ-rays and that the two kinds of radiation exhibit different sensitivities to the Tl concentration [14,15].

The results of our standardized prescans are displayed in Fig. 13. The histogram shows the number of scanned crystals, obtained from different companies, as a function of maximum detected scintillation uniformity. Crystals obtained from one supplier (a) were grown with the Czochralski technique [16,17]; crystals obtained from three other suppliers (b-d) were grown with the Stockbarger-Bridgman technique [17,18]. Crystals grown with the Czochralski technique exhibited, on average, more uniform scintillation efficiencies than crystals grown with the Stockbarger-Bridgman technique. Quality differences between different suppliers using the Stockbarger-Bridgman technique may not be significant since only a limited number of crystals were scanned for each supplier. (The number of crystals scanned from each supplier

is given in parentheses in Fig. 13.) Furthermore, some differences are expected to result from different ways of cutting the 2"X1.5"X1" crystals from the ingot, since Tl concentration gradients build up largely in the vertical crystal growth direction. Our standard scan of the 1.5"X2.0" face of each crystal should then reveal an especially large gradient of the scintillation efficiency when the 2" long side was cut parallel to the vertical growth direction of the ingot. Selective cuts of some crystals from various locations of the ingot and with different orientations with respect to the crystal growth direction provided supporting evidence for the relationship between the Tl concentration and the uniformity of scintillation response. For most of the crystals, such detailed information was not available to us.

6. Fabrication of Scintillator Foils

Scintillator foils were spun [19,20] from Betapaint, Bicron BC-498X plastic scintillator dissolved in xylene. The original solution was ordered with a 40% weight ratio of solute to solvent. It was then diluted by adding xylene until the solution had the desired viscosity of 20-30 poise.

The viscosity was determined by measuring the terminal speed, v, of a steel ball sinking in a glass tube filled with a sample of Betapaint. Correcting Stoke's Law for the finite diameter of the glass tube gives the following expression for the viscosity [21]:

$$\eta = \frac{2gr^2(\rho_n-\rho)}{9v}\left[1-2.104\left(\frac{r}{R}\right)+2.09\left(\frac{r}{R}\right)^3-0.95\left(\frac{r}{R}\right)^5\right] . \qquad (2)$$

Here, η denotes the viscosity, r and R are the diameters of the steel ball and the glass tube, g is the gravitational acceleration, and ρ_0 and ρ are the densities of the steel ball and the Betapaint, respectively.

For the fabrication of scintillator foils, a glass plate of 23 cm diameter was mounted horizontally on a small platform connected to the drive of an electrical motor which allowed spinning of the plate about its center at a preselected speed. To facilitate the removal of spun foils the glass plate was covered successively with metasilicate solution and Teepol 610 and then wiped to leave only a thin film of the releasing agents on the glass substrate. An appropriate amount of beta paint was poured on the center of a glass plate. In order to provide rapid spreading of the initial solution, the plate was spun at an enhanced speed for the first few seconds until the entire plate was covered with Betapaint. Following this rapid startup, the glass plate was spun at the preset rotational frequency for a duration of approximately 4 min until a solid foil had formed. After spinning, the glass plate was stored in a flow of dry nitrogen for a duration of about eight hours. The foil was then peeled from the glass plate, mounted on a frame, and placed in a dry nitrogen atmosphere for another 24 hours to allow further evaporation of residual xylene.

We obtained good and reproducible results by using more dilute solutions and spinning at lower rotational frequencies than described in ref. [20]. A number of measurements were performed to determine the relation between rotational frequency and foil thickness in this operating range. The results of these measurements are shown in Fig. 14. For each foil, thickness and homogeneity were determined by scanning the foil in vacuum with a collimated ^{228}Th α-source, and measuring the energy of the transmitted α- particles in a calibrated silicon detector. The energy loss in the foil was then converted to

an areal density according to ref. [22]. The spun foils were uniform in thickness to within typically 1-2% over an area of 7×7 cm^2. Scintillator foils used for instrumenting the Miniball in its present configuration were selected to have a thickness of 4.0 ± 0.12 mg/cm^2.

We have explored the light collection efficiency for scintillator foils placed with and without optical cement on the front faces of the CsI(Tl) scintillators. Considerable effort was spent on developing a technique which provides an optically clear glue bond of minimum thickness between the plastic scintillator foil and CsI(Tl) crystal. Best results were obtained with Epo-tek 301 which has a low viscosity of 1 poise and a curing time of 1 day. A thin layer of the epoxy was distributed on the scintillator foil by spin coating. By means of a thin rubber pad and a weight, the epoxy coated foil was pressed onto the CsI(Tl) crystal in vacuum and cured in a clean and dry nitrogen atmosphere. The pressure applied by the weight was typically 13 kPa. Glue layers of 300-500 $\mu g/cm^2$ areal density were achieved, with nonuniformities of the order of 50%.

We investigated the position dependence of the light collection efficiency for phoswich detectors prepared with and without glue bonds between the plastic scintillator foil and the CsI(Tl) crystal, by measuring the response at various locations on the front face (labelled 1 through 11 in Fig. 15). The upper and lower panels in Fig. 15 show the relative variations of the plastic scintillator response (integrated over the time interval Δt_{fast}= 0-50 ns) and the fast CsI(Tl) component (integrated over the time interval Δt_{slow}= 60-400 ns) for α-particles sampling different locations of a phoswich fabricated with (upper panel) and without (lower panel) a glue bond between the two scintillators. Both detectors have sufficient uniformity of response to provide good

particle identification (see also Sect. 8). In this bench test, a better uniformity of response was obtained for the phoswich without glue bond. Somewhat larger (but still tolerable) fluctuations are observed when a glue bond is applied. The observed fluctuations can be attributed to thickness variations of the glue layer which cause variations in energy deposition in the stopping CsI(Tl) scintillator (see open points in the top panel). Since some of the CsI(Tl) signal overlaps in time with the fast plastic scintillator signal, a correlated modulation appears in the charge integrated by the fast time gate. For more energetic particles, this effect should be less important as the energy loss in the glue layer decreases.

The fabrication of phoswich detectors without glue bond has the advantage of allowing changes in scintillator foil thickness to be made relatively easily. Glued phoswich detectors, on the other hand, are mechanically more rugged. In our test runs, improved particle identification was obtained with glued phoswich detectors (see Sect. 8). However, these improvements do not appear to be compelling enough to justify the initial use of glue bonds in the Miniball array.

7. Data Acquisition Electronics

Figure 16 shows a block diagram of the data acquisition electronics. The anode current from the photomultipliers is split via passive splitters into into the "fast", "slow", "tail", and "trigger" branches of relative amplitudes $I_{fast}:I_{slow}:I_{tail}:I_{trig} \approx 0.82:0.04:0.04:0.1$. The "slow" and "tail branches are connected directly from the splitter to their respective fast encoding readout analog-to-digital converters (FERAs). The gates for the "slow" and "tail" FERAs are 400 ns and 2 µs wide and open 200 ns and 2 µs after the leading edge of the linear signal, respectively. For the "fast" branch, a linear gate is

inserted between the passive splitter and the "fast" FERA. This linear gate allows the individual gating of each "fast" channel which cannot be achieved with the common gate FERAs (see also the discussion in Sect. 8). The linear gate is opened 5 ns prior to the leading edge of the linear signal and for a duration of 35 ns. The "fast" FERA is gated by a common gate of 100 ns width which begins approximately 35 ns prior to the leading edge of the linear input signal. The trigger branch, I_{trig}, is re-amplified by a fast amplifier and fed into a leading edge discriminator module, the output of which provides the stop signal for the time-to-FERA-converter and opens the linear gate for the "fast" channel.

Each discriminator module provides a sum output for its 16 channels. The amplitude of this sum signal is proportional to the number of channels which have triggered. By setting a discriminator level on the linear addition of all discriminator sum outputs, a simple multiplicity trigger is obtained.

In order to reduce dispersive losses for the fast anode current pulse representing the response of the plastic scintillator, the data acquisition electronics is located close to the measurement station. Discriminator thresholds and photomultiplier gains are adjusted via remote computer control. Remote inspection of each detector signal is also possible by using the sum output of the linear gate modules and selectively masking the discriminators.

8. Particle Identification

The particle identification resolution of various phoswich detectors was tested for fragments emitted at about $\Theta_{lab} \approx 35°$ in the $^{40}Ar+^{197}Au$ reaction at E/A=35 MeV. All data were taken with the standard electronics setup described in the previous section. Part (a) of Fig. 17 shows a two-dimensional plot of

the "fast" versus the "slow" charge integration parameters for a phoswich consisting of a 4 mg/cm^2 scintillator foil glued to the CsI(Tl) crystal. Elemental identification up to Z=18 is achieved over a considerable dynamical range of particle energies. Part (b) of the figure shows a linearized presentation of these data which is more suitable to display the resolution of the device. From such a linearized presentation, projections on the particle identification axis can be generated which show the particle identification resolution in a more quantitative form.

Spectra projected on the particle identification axis are shown in Fig. 18. Part (a) of the figure shows the projection of the data displayed in Fig. 17; part (b) show the result for a phoswich using a 4 mg/cm^2 scintillator foil without glue bond. Better resolution is obtained by using a glue bond between the scintillator foil and the CsI(Tl) crystal. Additional improvements in particle identification resolution can be achieved by increasing the thickness of the scintillator foil. For a specific experiment, the benefits of improved particle identification resolution due to an increase in scintillator foil thickness must be weighed against the ensuing higher energy threshold. We have also explored the use of thinner foils and found that the resolution deteriorates rapidly for scintillator foils thinner than 3 mg/cm^2. For most purposes, particle identification provided by foils of 4 mg/cm^2 thickness is satisfactory.

The use of thin scintillator foils in phoswich detectors for particle identification is complicated by the fact that the fast plastic scintillator signal is superimposed on the rising signal from the CsI(Tl) scintillator. Good particle identification via direct charge integration depends critically on well defined integration times. Electronic walk introduced by leading edge

discriminators changes the detailed shape of a particle identification line in the "fast" versus "slow" matrix, but it has only minor effects on the separation between adjacent particle identification lines. Time jitter in the integration gate, however, does have an adverse effect on the particle identification resolution, since it produces fluctuations in the amount of CsI(Tl) scintillation integrated by the fast time gate. If the fast component is integrated by ADCs with a common gate mode, loss in resolution will occur whenever there is a time jitter between gates provided by different channels. Loss in resolution will be inevitable when more than two detected particles with different flight times are converted in separate channels of a common gate ADC. The problem can be avoided by introducing linear gates into the "fast" channel which are individually opened (see Fig. 16) or, alternatively, by employing passive filter networks of good quality [23].

Figure 19 illustrates the sensitivity of the particle identification to time jitter in the integration gate for the "fast" channel. The solid curves correspond to the centers of selected particle identification lines in the "fast" versus "slow" matrix (see, e.g. Fig. 17). The dashed curves show how these particle identification lines are shifted when the gate of the "fast" ADC arrives two 2 ns later in time. (In these two measurements, the gate width was kept constant.) Even a 2 ns time jitter in the "fast" gate is sufficient to mix the particle identification lines of neighboring elements in the "fast" versus "slow" matrix.

Identification of hydrogen and helium isotopes is obtained by standard pulse shape discrimination techniques which make use of the fact that the temporal decay of the CsI(Tl) light output depends on the ionization density of the detected particles [24-26]. As an example, Fig. 20 shows the particle

identification obtained from a two-dimensional matrix of the "slow" versus "tail" parameters. Good particle identification is obtained over a broad range of energies. In these spectra, not all particles are stopped in the CsI(Tl) crystal. The effects of particles "punching through" the detectors are clearly visible. Particles not stopped in the CsI(Tl) crystal can still be separated by atomic number.

9. Summary

We have constructed a compact phoswich detector array for the detection of multi-fragment emission from highly excited nuclear systems in heavy ion induced reactions. The array is designed to operate in vacuum. It consists of 188 individual phoswich detectors arranged in 11 rings coaxial with the beam axis. The granularity of the device increases towards more forward angles. Each phoswich detector consists of a 4 mg/cm^2 (40 μm) thick plastic scintillator foil and a 2 cm thick CsI(Tl) crystal. By selecting CsI(Tl) crystals of good scintillation uniformity and homogenous scintillator foils, and by making efforts to preserve and cleanly integrate the fast anode signal containing the plastic scintillator response, good element identification up to $Z \approx 18$ was obtained. Detectors utilizing a thin glue bond between the plastic scintillator foil and CsI(Tl) crystal gave slightly better particle identification resolution than detectors without glue bonds. However, since glue bonds increase the energy threshold and make changes of scintillator foil thickness very time and labor intensive, the argument for glued phoswich detectors does not appear compelling.

Acknowledgements

We wish to thank D.G. Sarantites, L.G. Sobotka, D. Swan, J. Telfer, and J. Yurkon for helpful discussions. Advice from M. Maier and J. Vincent on electronics questions is gratefully acknowledged. The continued support from the entire NSCL staff and the excellent work of the NSCL mechanical workshop are highly appreciated. This work is based upon work supported by the National Science Foundation under Grant numbers PHY-86-11210 and PHY-89-13813. WGL acknowledges the receipt of U.S. Presidential Young Investigator Award and NC acknowledges partial support by the FAPESP, Brazil.

References

1. W.G. Lynch, Ann. Rev. Nucl. Part. Sci., 37 (1987) 493; and references contained therein.

2. J.E. Finn, S. Agarwal, A. Bujak, J. Chuang, L.J. Gutay, A.S. Hirsch, R.W. Minich, N.T. Porile, R.P. Scharenberg, B.C. Stringfellow, and F. Turkot, Phys. Rev. Lett. 49 (1982) 1321.

3. L.P. Csernai and J.I. Kapusta, Phys. Reports 131 (1986) 223.

4. G. Bertsch and P.J. Siemens, Phys. Lett. 126B (1983) 9.

5. J.A. Lopez and P.J. Siemens, Nucl. Phys. A431 (1984) 728.

6. A. Vicentini, G. Jacucci, and V.R. Pandharipande, Phys. Rev. C31 (1985) 1783.

7. R.J. Lenk and V.R. Pandharipande, Phys. Rev. C34 (1986) 177.

8. T.J. Schlagel and V.R. Pandharipande, Phys. Rev. C36 (1987) 162.

9. K. Sneppen and L. Vinet, Nucl. Phys. A480 (1988) 342.

10. D.G. Sarantites, L.G. Sobotka, T.M. Semkow, V. Abenante, J. Elson, J.T. Hood, Z. Li, N.G. Nicolis, D.W. Stracener, J. Valdes, and D.C. Hensley, Nucl. Instr. and Meth. A264 (1988) 319.

11. D. Drain, A. Giorni, D. Hilscher, C. Ristori, J. Alarja, G. Barbier, R. Bertholet, R. Billerey, B. Chambon, B. Cheynis,, J. Crançon, A. Dauchy, P. Désesquelles, A. Fontenille, L. Guyon, D. Heuer, A. Llères, M. Maurel, E. Monnand, H. Nifenecker, C. Pastor, J. Pouxe, H. Rossner, J. Saint-Martin, F. Schussler, P. Stassi, M. Tournier, and J.B. Viano, Nucl. Instr. and Meth., to be published.

12. W.G. Gong, Y.D. Kim, G. Poggi, Z. Chen, C.K. Gelbke, W.G. Lynch, M.R. Maier, T. Murakami, M.B. Tsang, H.M. Xu, and K. Kwiatkowski, Nucl. Instr. and Meth. A268 (1988) 190.

13. W.G. Gong, N. Carlin, C.K. Gelbke, and R. Dayton, Nucl. Instr. and Meth. A287 (1990) 639.

14. J.B. Birks, The theory and practice of scinitllation counting (Pergamon Press, New York, 1964), p. 92.

15. W.W. Managan, IRE Trans. Nucl. Sci. NS-9,3 (1962) 8.

16. J. Czochralski, Z. Phys. Chem. 92 (1918) 219.

17. J.C. Brice, "The growth of crystals from the melt", (North Holland Publishers, Amsterdam, 1965).

18. P.W. Bridgman, Proc. Amer. Acad. Arts. Sci. 60 (1925) 305.

19. D. Meyerhofer, J. Appl. Phys. 49 (1978) 3993.

20. E. Norbeck, T.P. Dubbs, and L.G. Sobotka, Nucl. Instr. and Meth. A262 (1987) 564.

21. A. Dinsdale and F. Moore, Viscosity and its Measurement (Chapman-Hill, London, 1962).

22. U. Littmark and J.F. Ziegler, "Handbook of Range Distributions for Energetic Ions in All Elements", Volume 6 of "The Stopping and Ranges of Ions in Matter", edited by J.F. Ziegler, Pergamon Press, New York, 1980.

23. D.G. Sarantites and L.G. Sobotka, private communication.

24. R.S. Storey, W. Jack, and A. Ward, Proceedings of the Phys. Society 72 (1958) 1.

25. J.A. Biggerstaff, R.L. Becker, and M.T. McEllistrem, Nucl. Instr. and Meth. 10 (1961) 327.

26. J. Alarja, A. Dauchy, A. Giorni, C. Morand, E. Pollaco, P. Stassi, B. Billerey, B. Chambon, B. Cheynis, D. Drain, and C. Pastor, Nucl. Instr. and Meth. A242 (1986) 352.

Figure Captions

Fig. 1. Artist's perspective of the assembly structure of the Miniball 4π fragment detection array. For clarity, electrical connections, the light pulsing system, the cooling system, and the target insertion mechanism have been omitted.

Fig. 2. Half-plane section of the Miniball array. Individual detector rings are labelled 1 through 11; numbers of detectors per ring are given in parentheses; the polar angles for the centers of the rings are indicated. The dashed horizontal line indicates the beam axis.

Fig. 3. Front views of different detector shapes. The detectors are labelled by their ring number; numbers of detectors per ring are given in parentheses.

Fig. 4. Isometric view of the target insertion mechanism.

Fig. 5. Schematic of phoswich assembly of individual detector elements. The μ-metal shield covering the photomultiplier is not included.

Fig. 6. Photograph of photomultiplier assembly. The scintillator and the first matching light guide are removed. The ring glued to the μ-metal shield defines the alignment of the can housing the voltage divider. The can has been removed to expose the voltage divider.

Fig. 7. Schematic of the active voltage divider used for the Miniball detectors.

Fig. 8. Schematics of light pulser assembly and LED trigger circuit.

Fig. 9. Open points: gain variations of a CsI(Tl) photomultiplier assembly determined by measuring the detector response to 8.785 MeV α-particles; solid points: same data corrected for gain shifts in the off-line analysis by using information from the light pulser system.

Fig.10. Relative variation of scintillation efficiency measured for two parallel surfaces of a CsI(Tl) crystal by using a collimated α-source. The axes of the coordinate system are parallel to the sides of the scintillator; the coordinates are fixed with respect to the scintillator.

Fig.11. Variations of scintillation efficiency measured with a charge integrating ADC for two different time gates selecting the fast and slow components of scintillation for CsI(Tl).

Fig.12. Variations of scintillation efficiency detected with collimated α-particles of 8.785 MeV energy (solid points) and collimated γ-rays of 662 keV energy (open points). The left hand panel shows the measurement for a detector which was rejected. The right hand panel shows the measurement for a detector which was incorporated into the Miniball.

Fig.13. Maximum detected scintillation nonuniformity for crystals obtained from different suppliers. The number of crystals scanned for each supplier is given in parenthesis.

Fig.14. Relation between scintillator foil thickness and rotational frequency of spinning measured for solutions of Betapaint of different viscosity. The lines show fits with the power law expression, $t \propto \nu^{-\alpha}$.

Fig.15. Position dependent response of phoswich detectors with (upper panel) and without (lower panel) glue bond between plastic and CsI(Tl) scintillators. Solid and open points show charges integrated by the "fast" and "slow" time gates, Δt_{fast}=0-50 ns and Δt_{slow}=60-400 ns, respectively. The same foil and CsI(Tl) crystal were used in this test. Various positions sampling the entrance window are labelled 1-11.

Fig.16. Schematic diagram of the data acquisition electronics of the Miniball.

Fig.17. Particle identification obtained from two-dimensional "fast" vs. "slow" matrix for reaction products emitted at Θ_{lab}=35° for the $^{40}Ar+^{197}Au$ reaction at E/A=35 MeV; a scintillator foil of 4 mg/cm^2 areal density was used with a thin glue coupling to the CsI(Tl) crystal. (a) Matrix of raw data. (b) Linearized matrix. An intensity threshold of 2 counts per channel has been set.

Fig.18. Projections of linearized particle identification spectra for reaction products emitted in the $^{40}Ar+^{197}Au$ reaction at Θ_{lab}≈35° using phoswich detectors using scintillator foils of 4 mg/cm^2 thickness, (a) with and (b) without glue coupling between the scintillator foil and the CsI(Tl) crystal.

Fig.19. Sensitivity of particle identification to time shift of the "fast" charge integration gate. The solid and dashed lines show the loci of representative particle identification lines in the "fast" vs. "slow" identification matrix obtained for gates displaced by 2 ns with respect to each other.

Fig.20. Particle identification obtained from two-dimensional "slow" vs. "tail" matrix for reaction products emitted at $\theta_{lab}=35^{\circ}$ for the $^{40}Ar+^{197}Au$ reaction at E/A=35 MeV.

MSU-90-047

Fig. 1

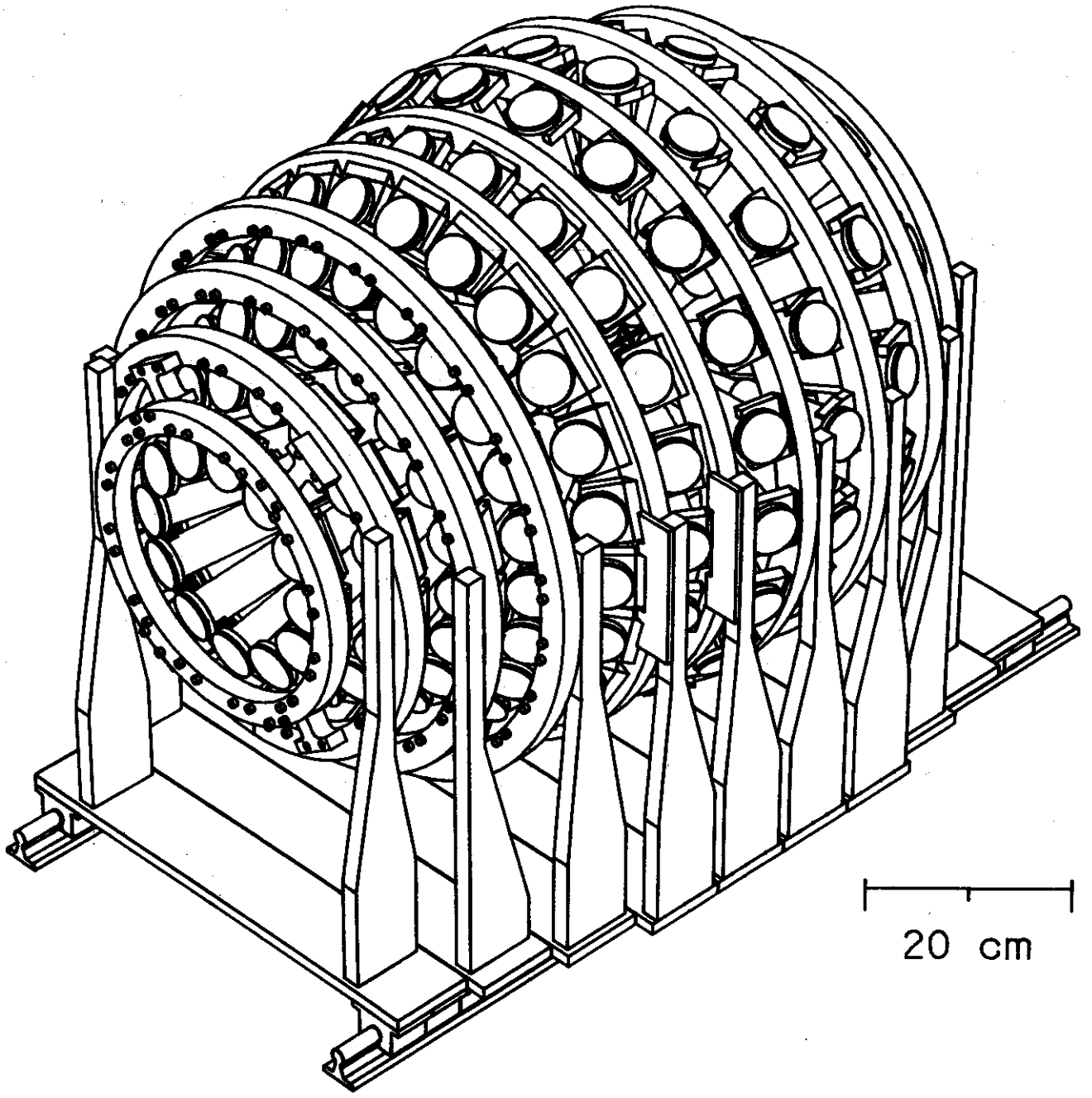

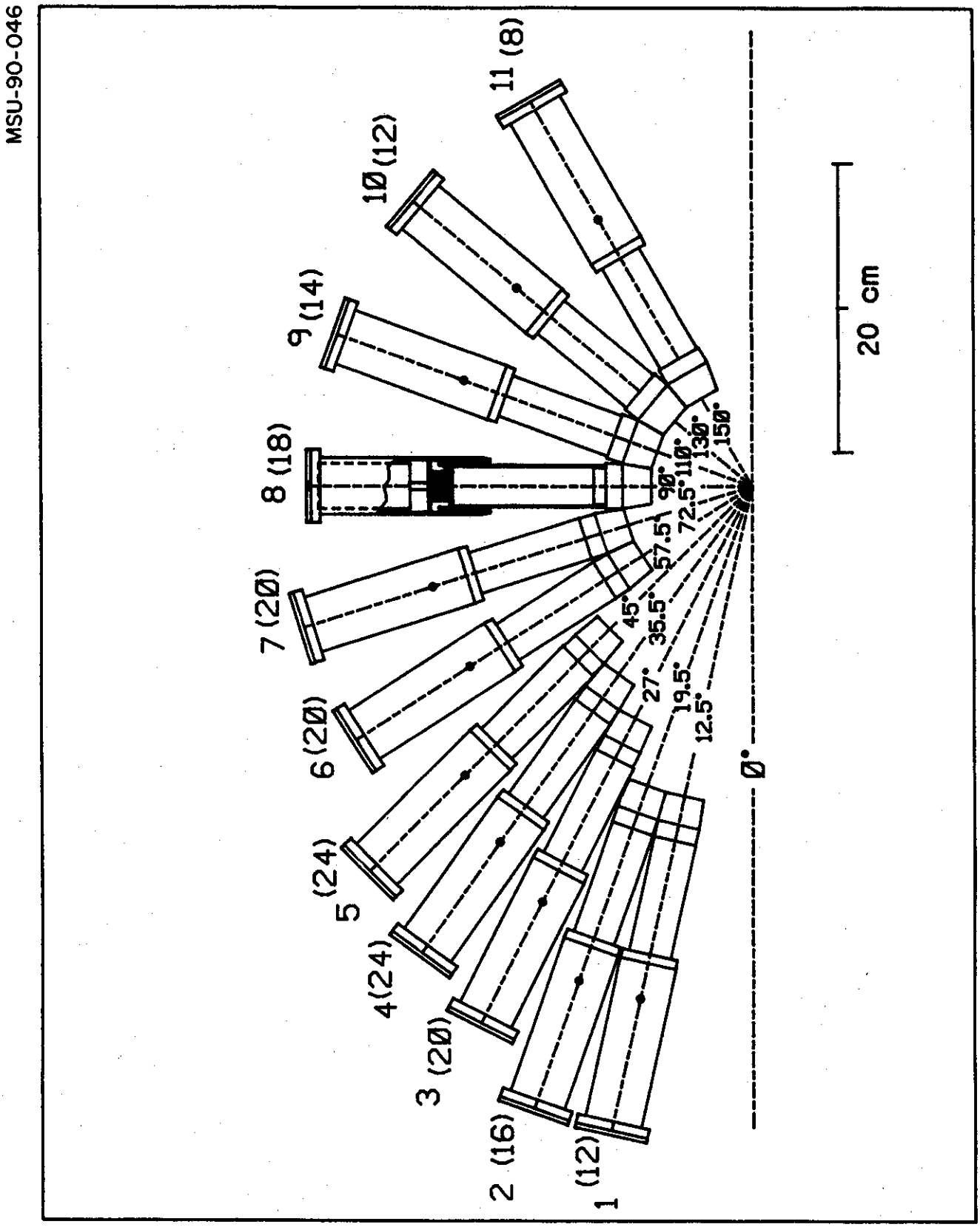
MSU-90-046
1 (12)
2 (16)
3 (20)
4(24)
5 (24)
6(20)
7(20)
8 (18)
9 (14)
10 (12)
11 (8)
0°
12.5°
19.5°
27°
35.5°
45°
57.5°
72.5°
90°
110°
130°
150°
20 cm

Fig. 2

Fig. 3

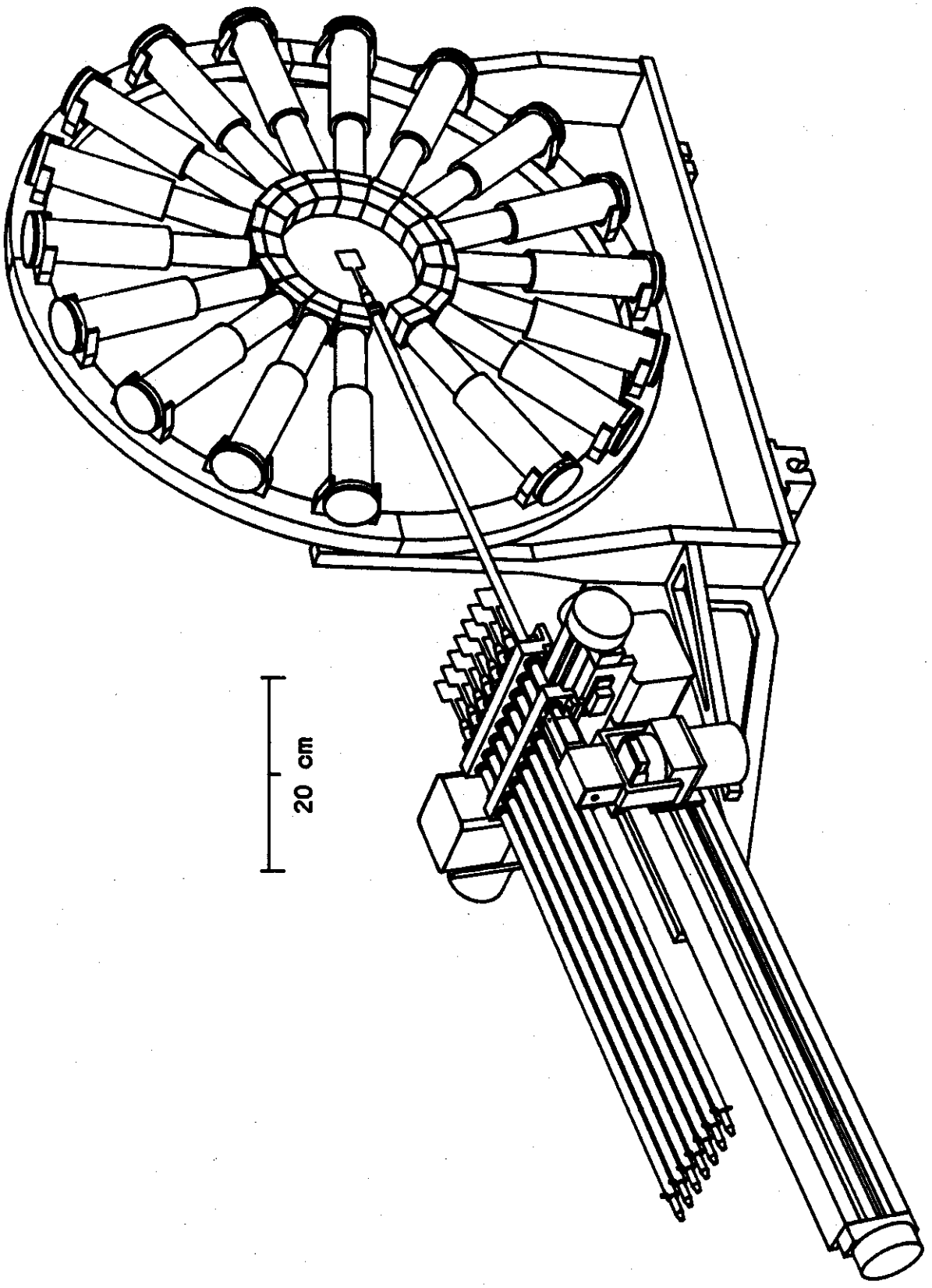

Fig. 4

MSU-90-031

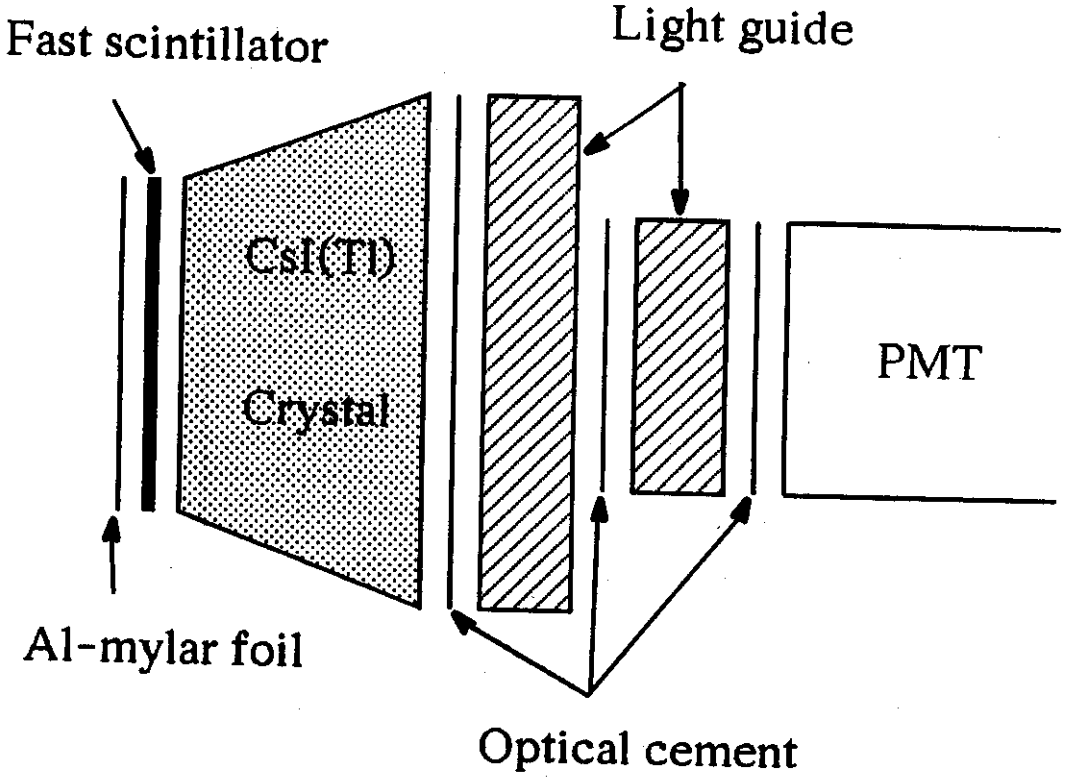

Fig. 5

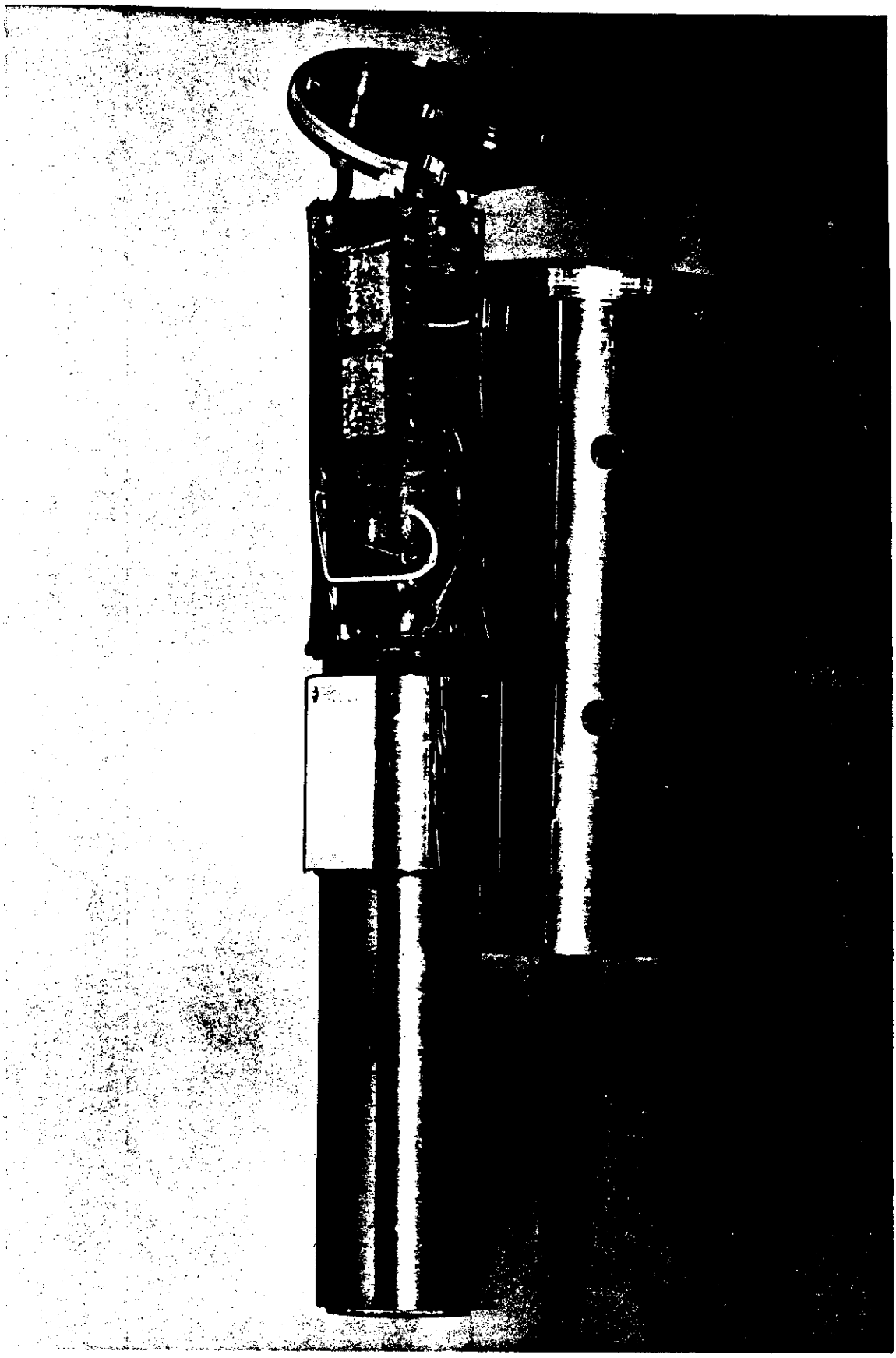

Fig. 6

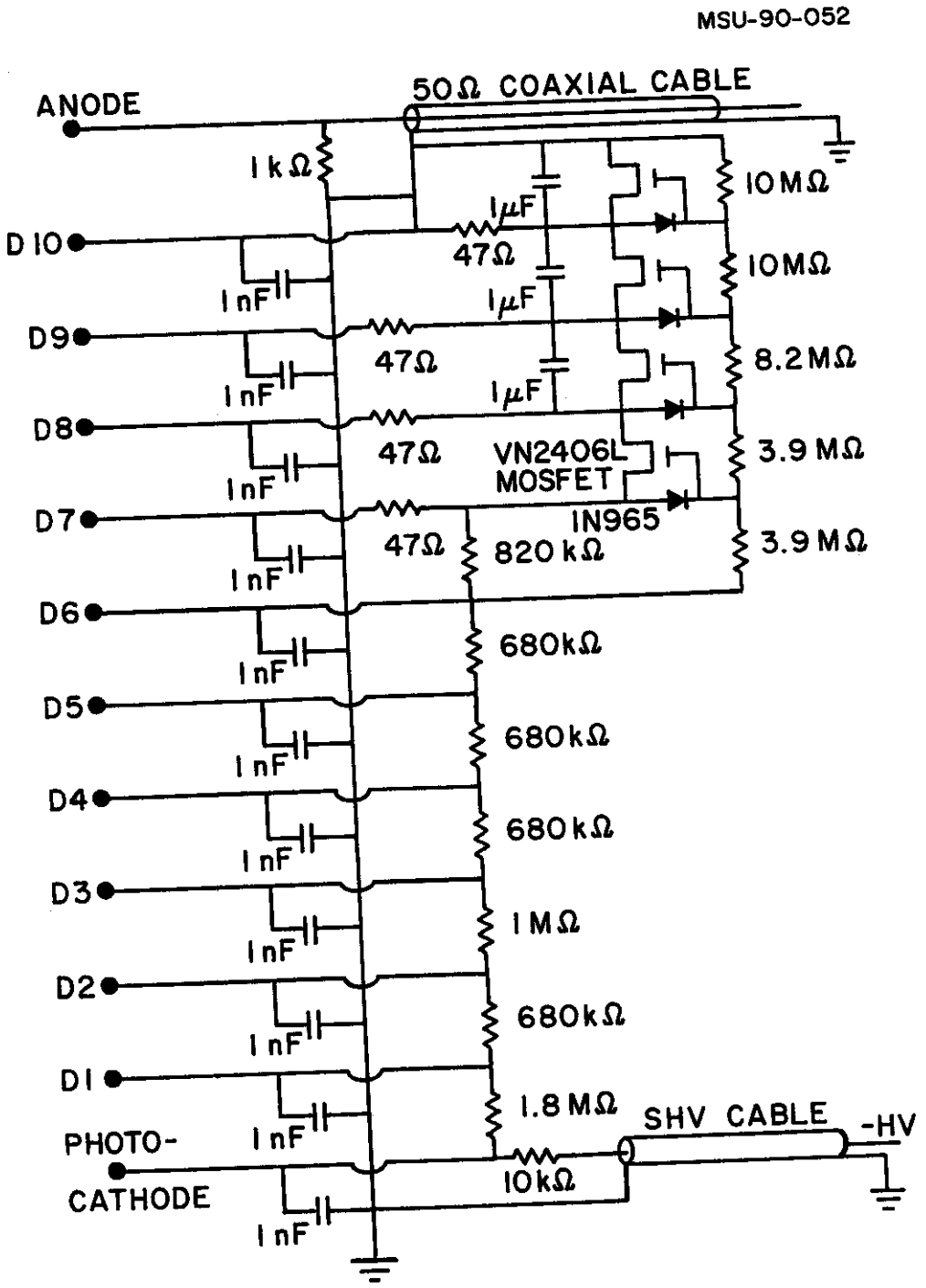
MSU-90-052
ANODE
50Ω COAXIAL CABLE
1kΩ
10MΩ
1μF
47Ω
D10
10MΩ
1nF
1μF
D9
47Ω
8.2MΩ
1nF
1μF
D8
47Ω
VN2406L
MOSFET
3.9MΩ
1nF
IN965
D7
47Ω
820kΩ
3.9MΩ
1nF
D6
680kΩ
1nF
D5
680kΩ
1nF
D4
680kΩ
1nF
D3
1MΩ
1nF
D2
680kΩ
1nF
D1
1.8MΩ
SHV CABLE
-HV
PHOTO-
1nF
10kΩ
CATHODE
1nF

Fig. 7

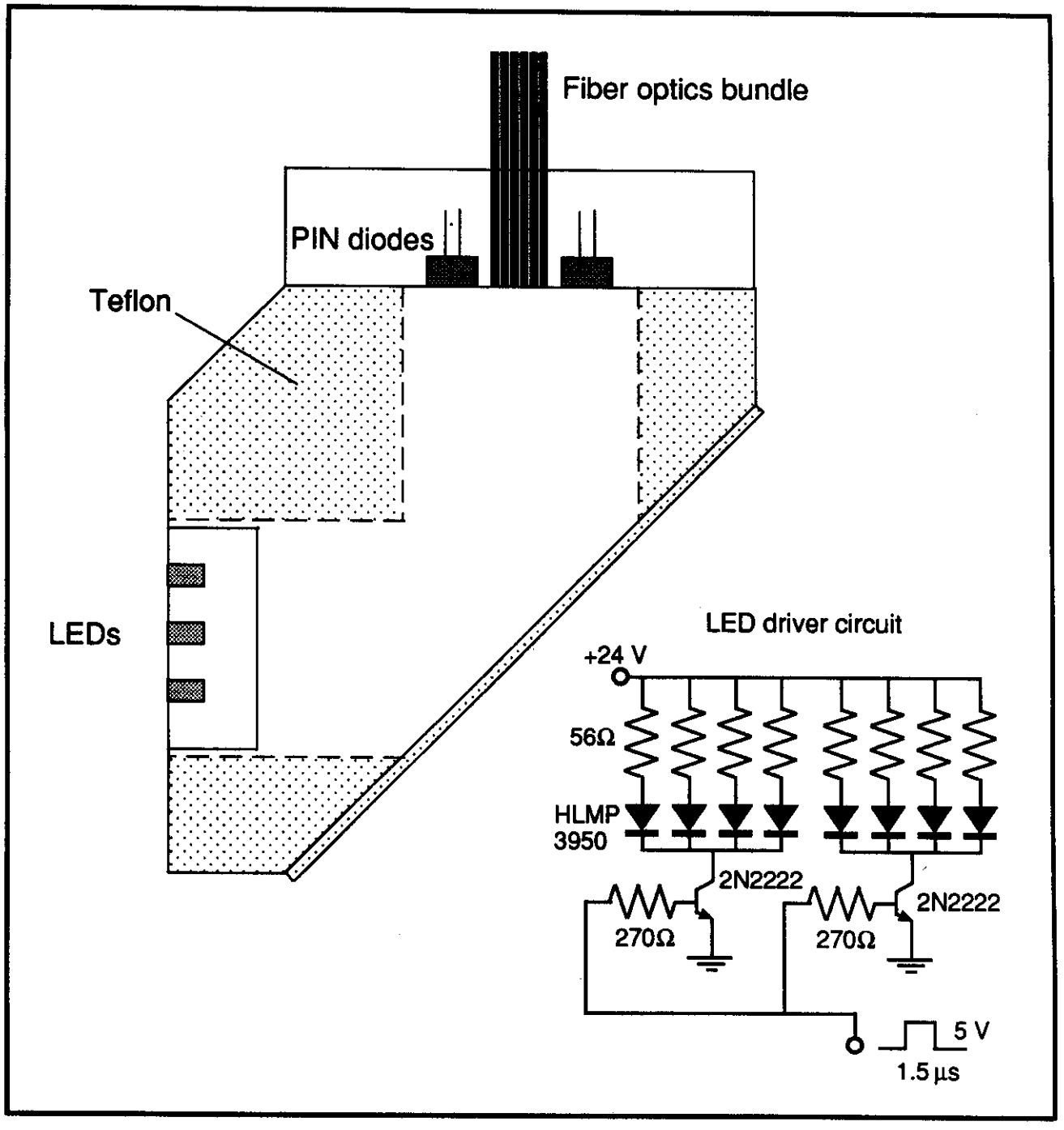
Fiber optics bundle
PIN diodes
Teflon
LEDs
LED driver circuit
+24 V
56Ω
HLMP
3950
2N2222
2N2222
270Ω
270Ω
5 V
1.5 µs

Fig. 8

Fig. 9

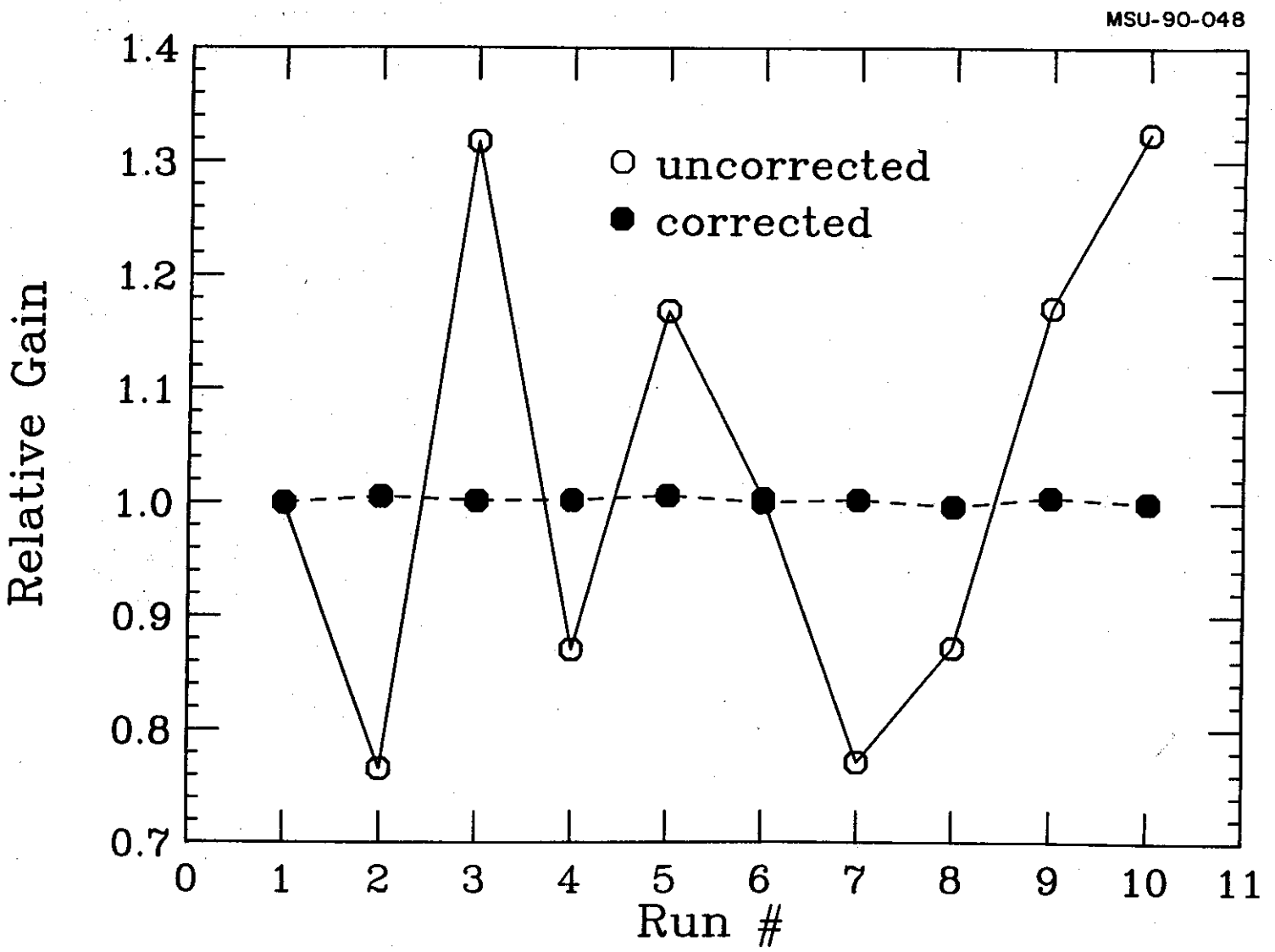
MSU-90-048
uncorrected
corrected
Relative Gain
Run #
1.4
1.3
1.2
1.1
1.0
0.9
0.8
0.7
0
1
2
3
4
5
6
7
8
9
10
11

Fig. 10

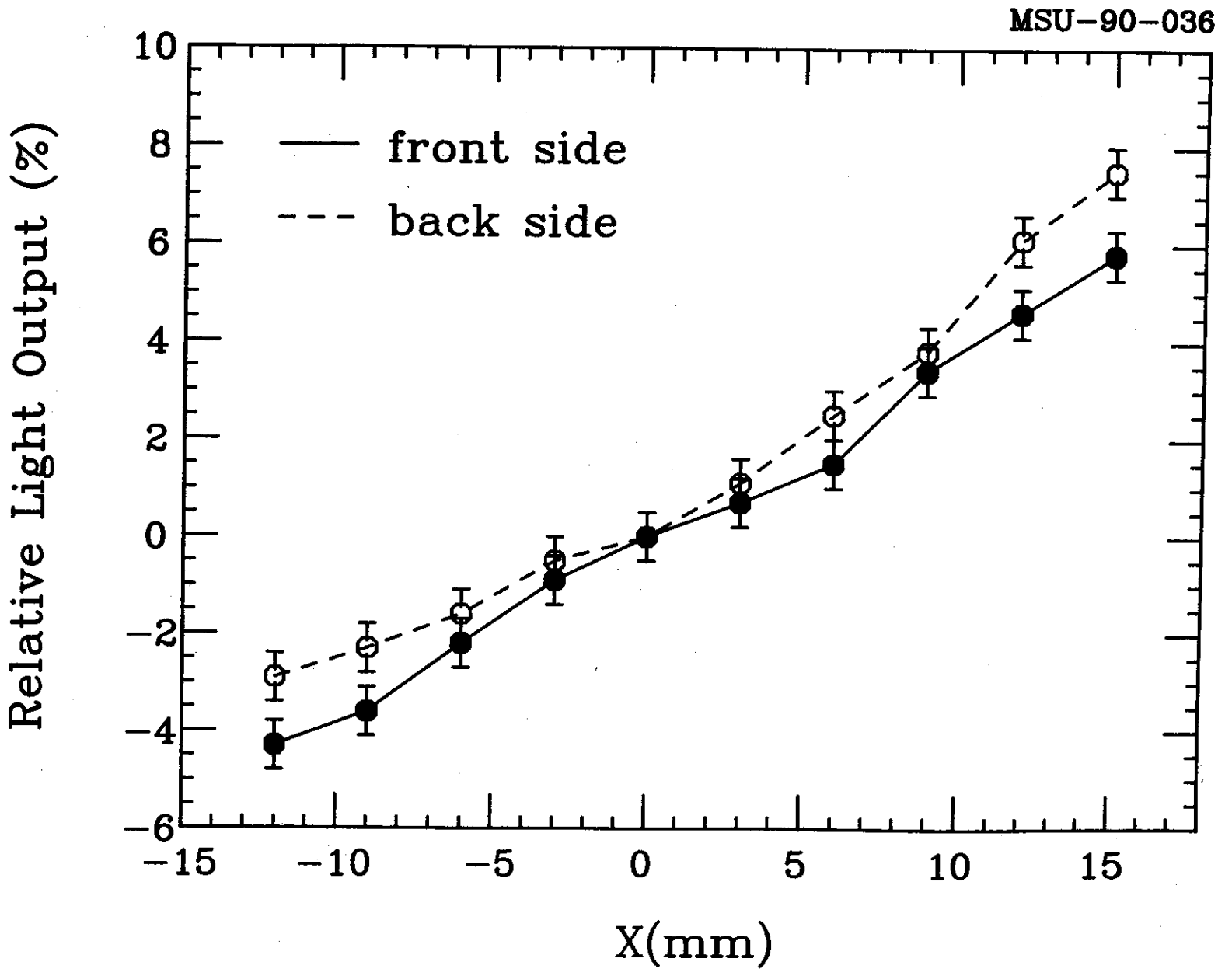
MSU-90-036
front side
back side
Relative Light Output (%)
X(mm)
10
8
6
4
2
0
−2
−4
−6
−15
−10
−5
0
5
10
15

Fig. 11

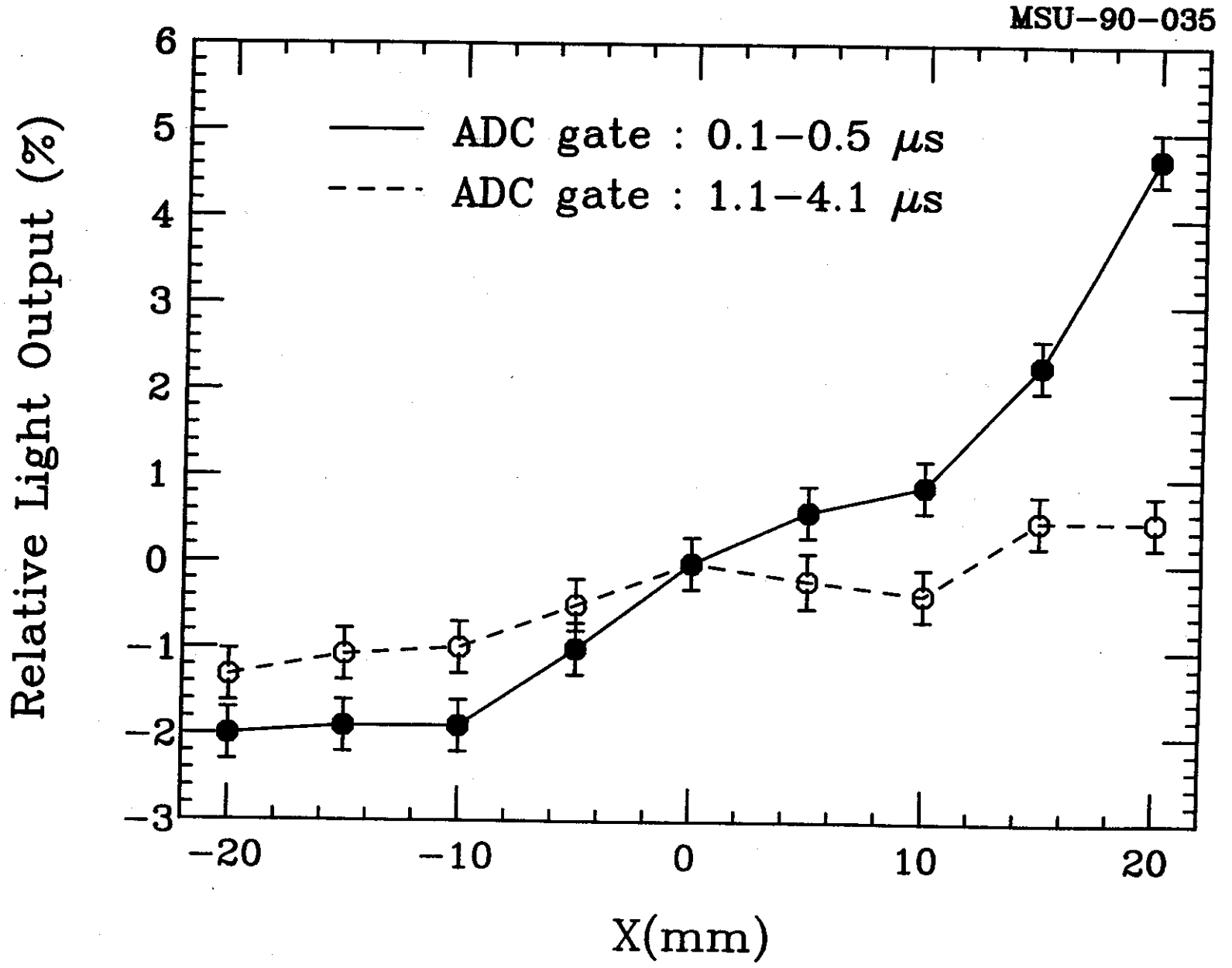
MSU-90-035
ADC gate : 0.1–0.5 μs
ADC gate : 1.1–4.1 μs
Relative Light Output (%)
X(mm)
6
5
4
3
2
1
0
−1
−2
−3
−20
−10
0
10
20

Fig. 1a

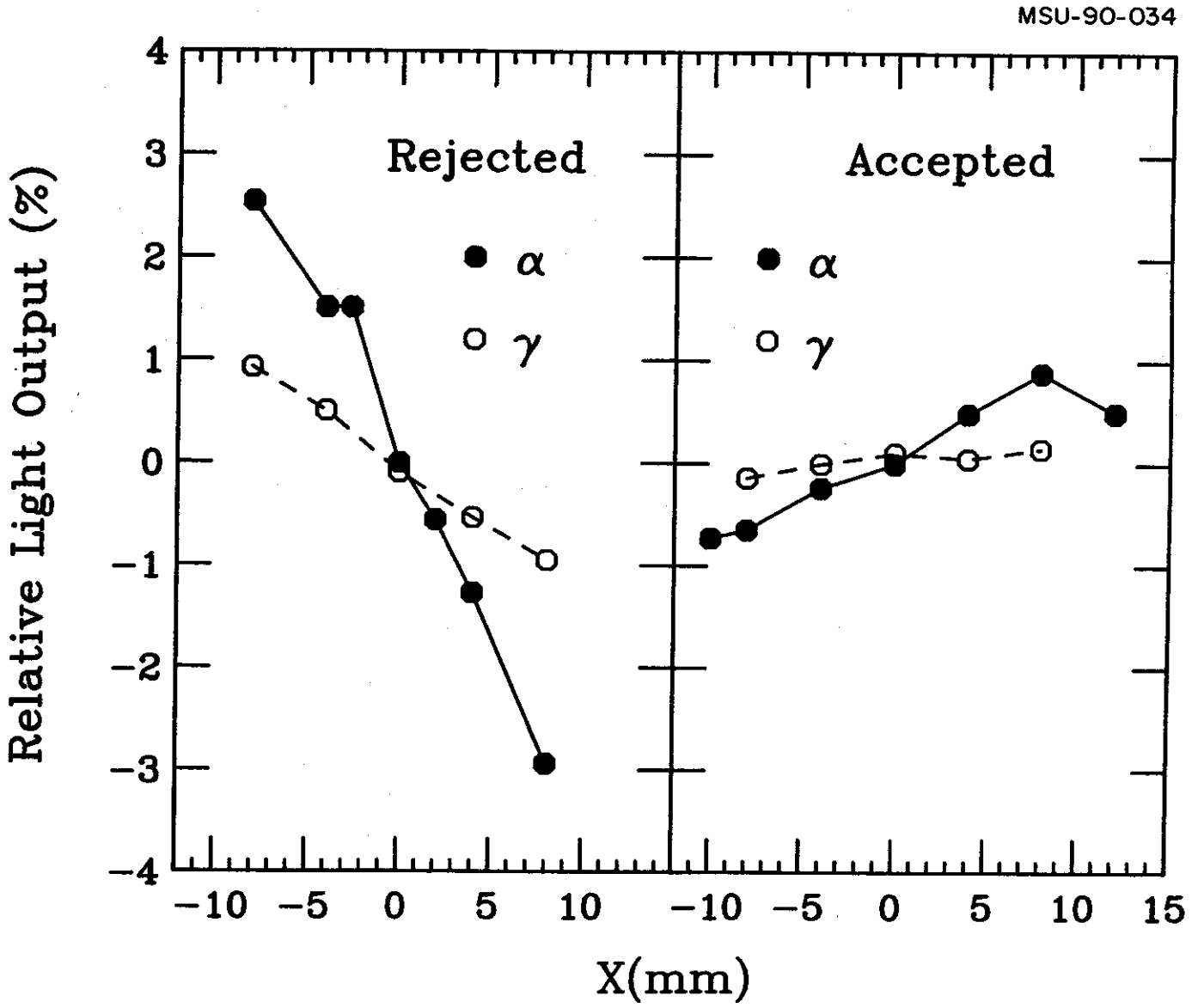
MSU-90-034
Rejected
Accepted
α
γ
α
γ
Relative Light Output (%)
X(mm)
4
3
2
1
0
−1
−2
−3
−4
−10
−5
0
5
10
−10
−5
0
5
10
15

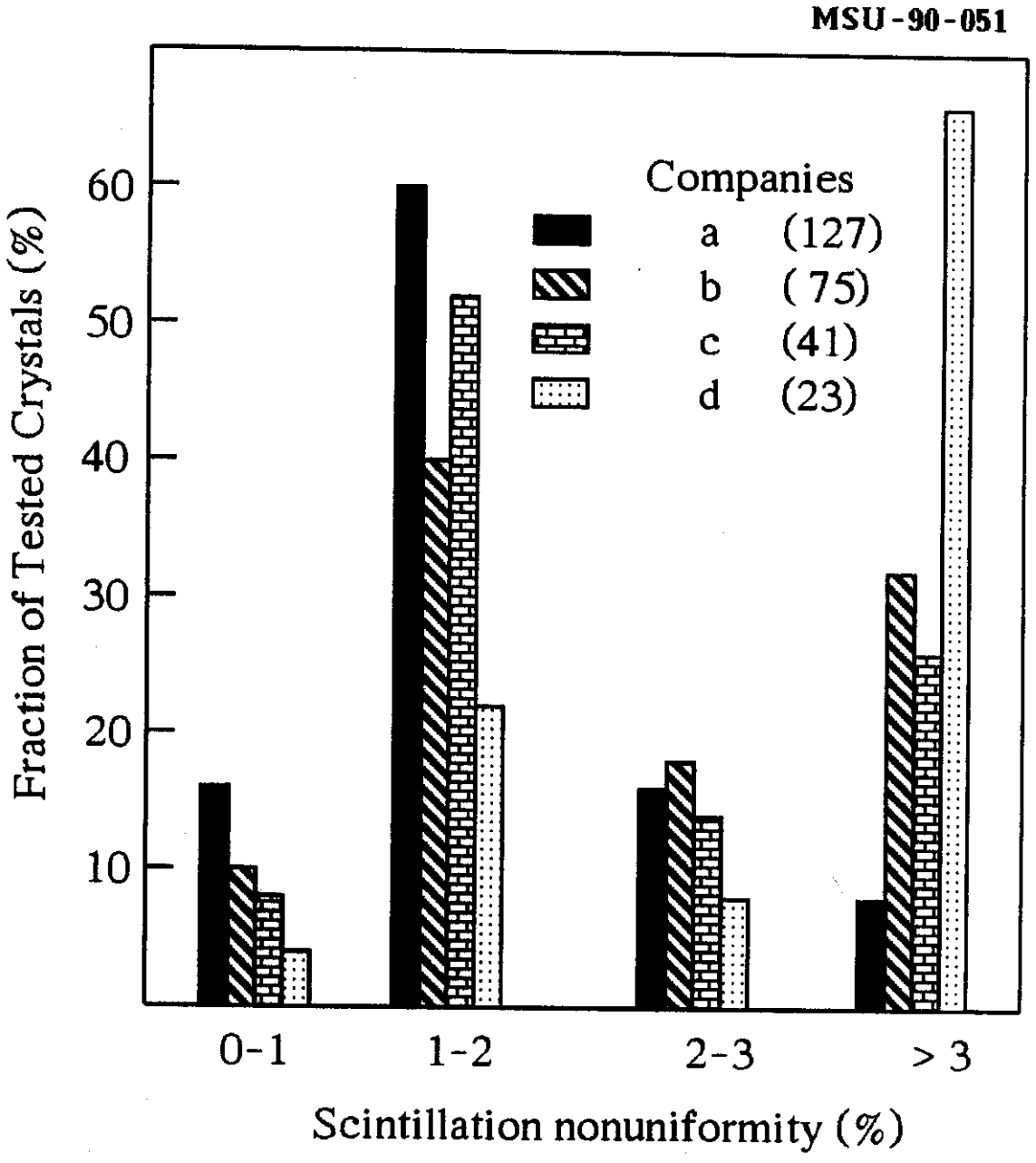
MSU-90-051
Companies
a (127)
b (75)
c (41)
d (23)
Fraction of Tested Crystals (%)
60
50
40
30
20
10
0-1
1-2
2-3
> 3
Scintillation nonuniformity (%)

Fig. 13

MSU-90-037
t ∝ ν^−α
α=0.67
η = 41 poise
α=0.55
η = 25 poise
ν (rpm)
200
300
400
500
600
2
3
4
5
6
7
8
τ (mg/cm²)

Fig. 14

Fig. 15

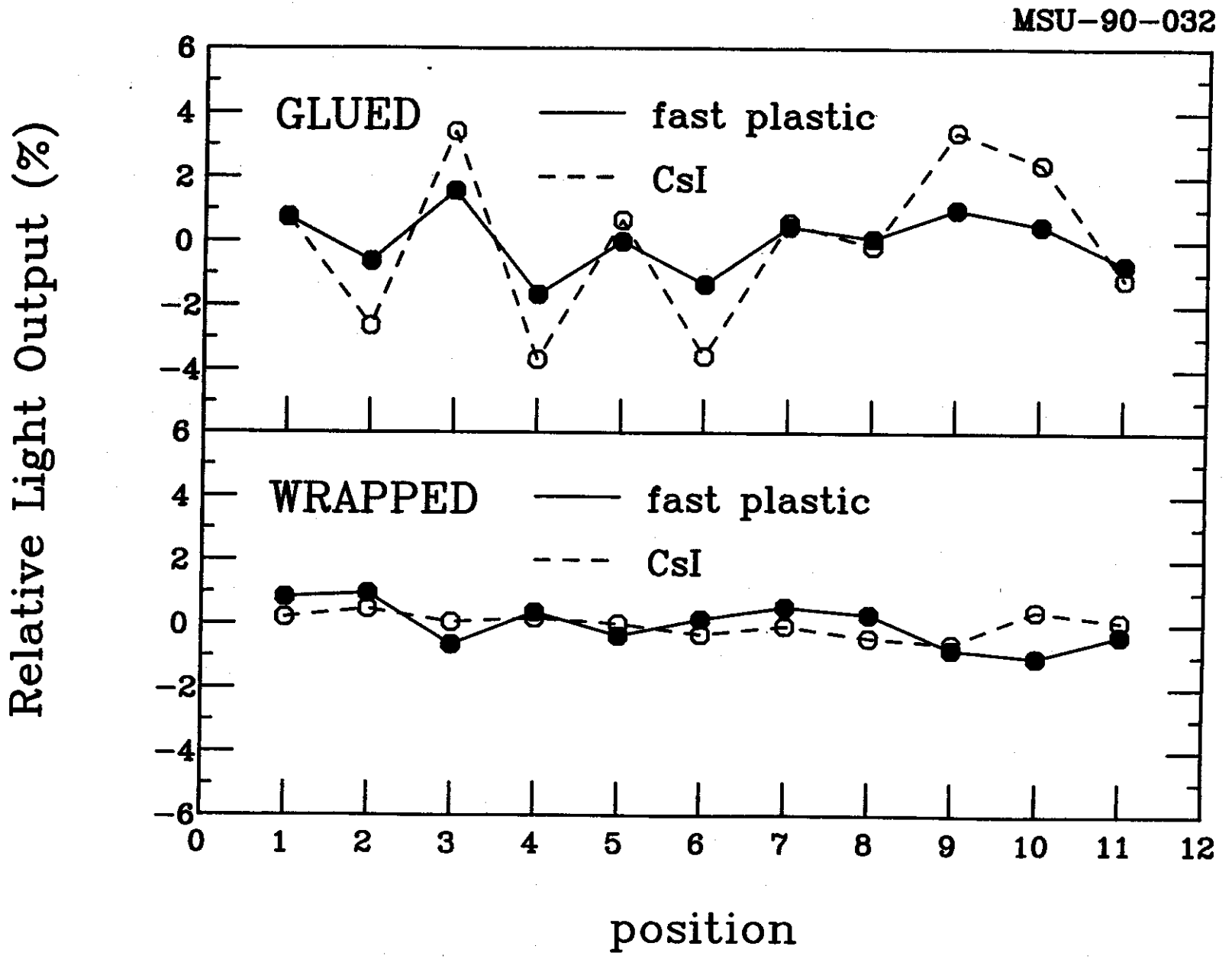
MSU-90-032
GLUED
fast plastic
CsI
WRAPPED
fast plastic
CsI
Relative Light Output (%)
position
6
4
2
0
-2
-4
-6
0
1
2
3
4
5
6
7
8
9
10
11
12

MSU - 90 - 053

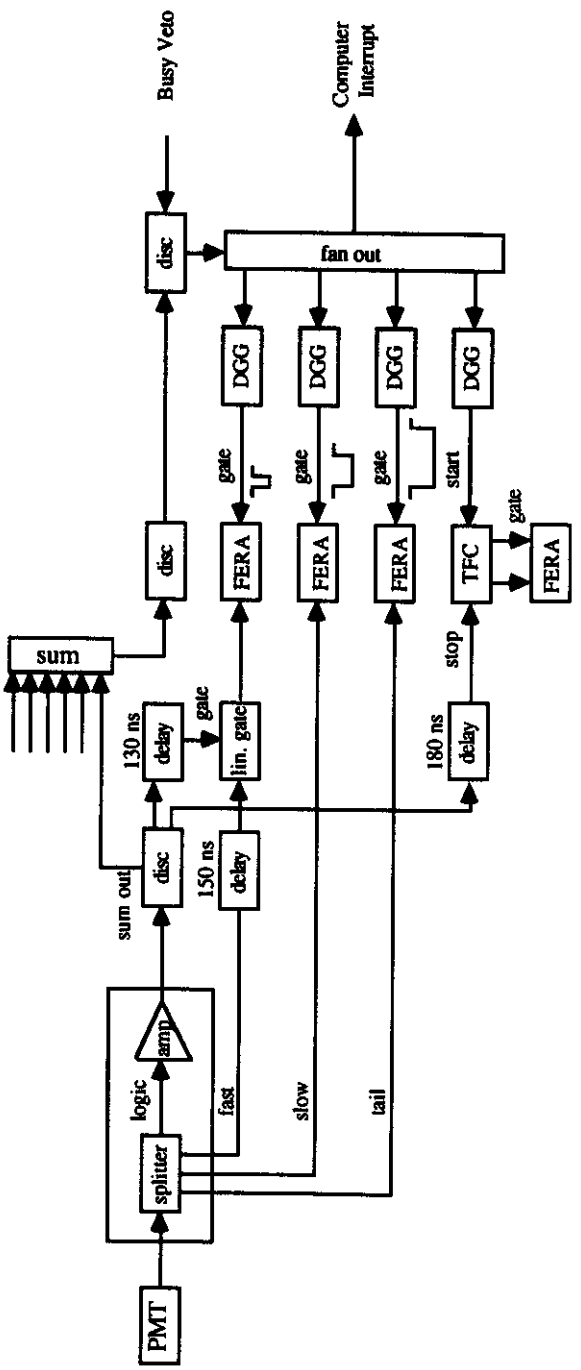

DGG - Delay and Gate Generator
FERA - Fast Encoding and Readout ADC
PMT - Photomultiplier Tube
TFC - Time-to-FERA Converter

Fig. 16

MSU-90-050

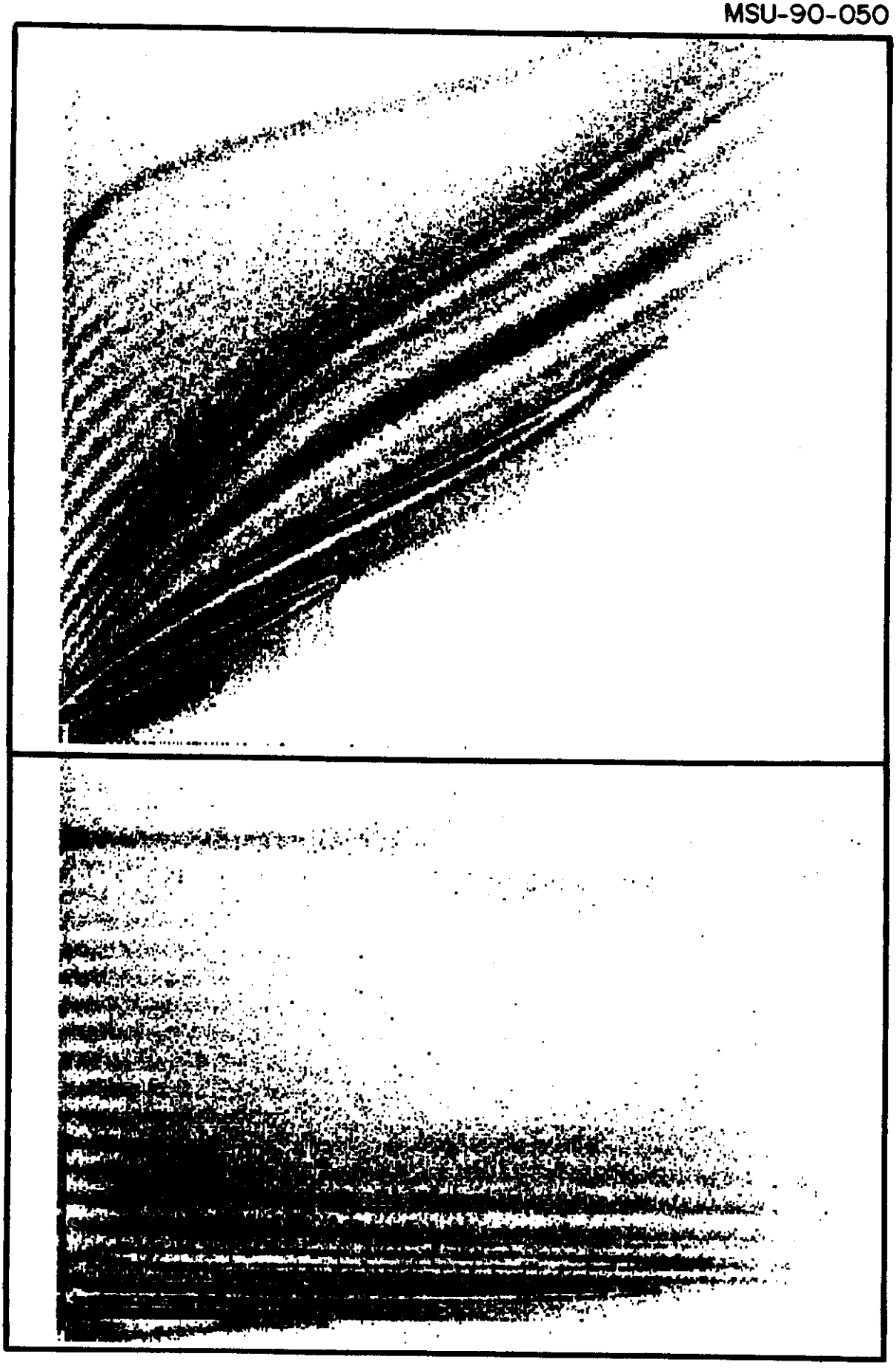

Fig. 17

Fig. 8)

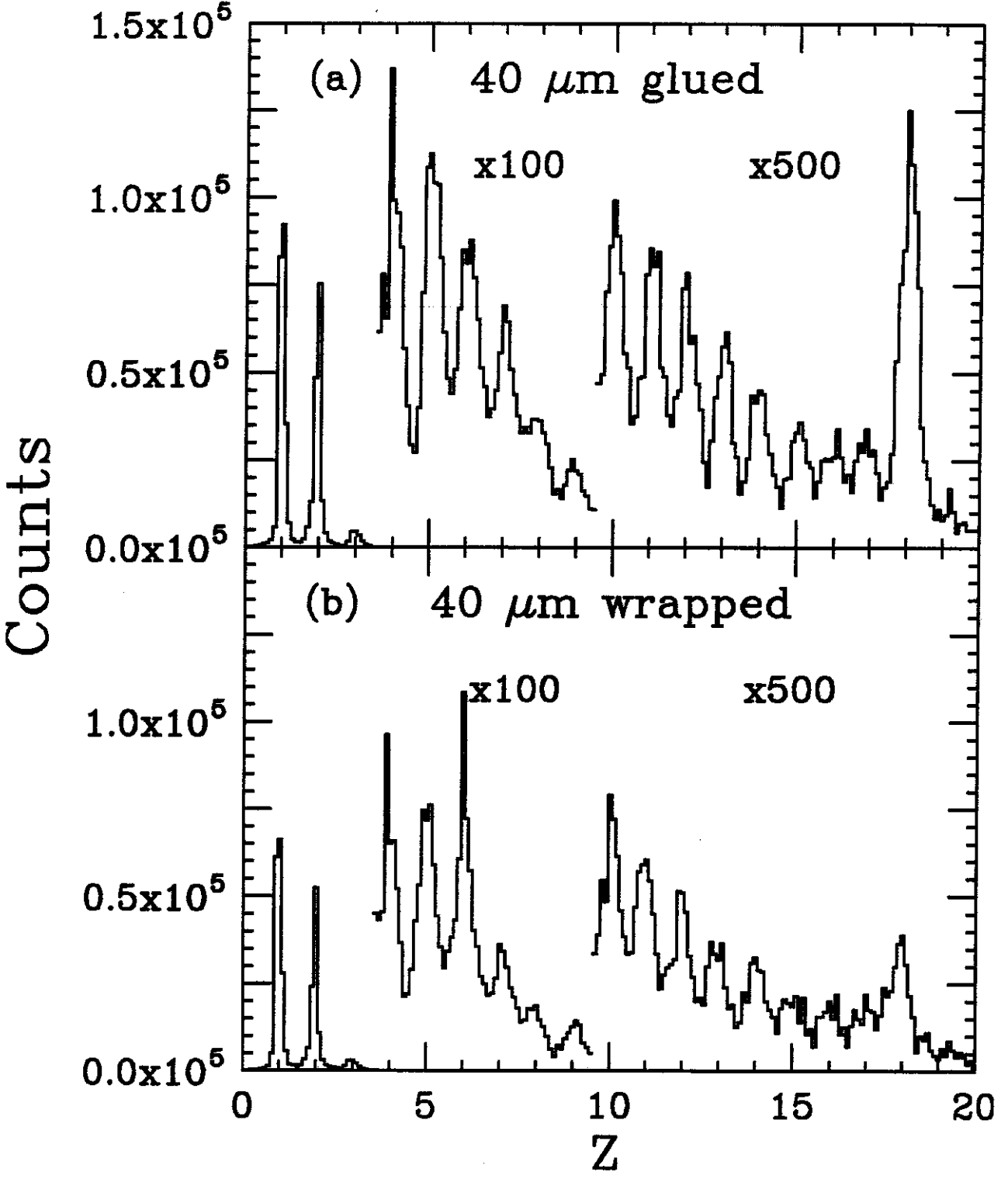
(a) 40 μm glued
x100
x500
(b) 40 μm wrapped
x100
x500
Counts
Z
1.5x10^5
1.0x10^5
0.5x10^5
0.0x10^5
0
5
10
15
20

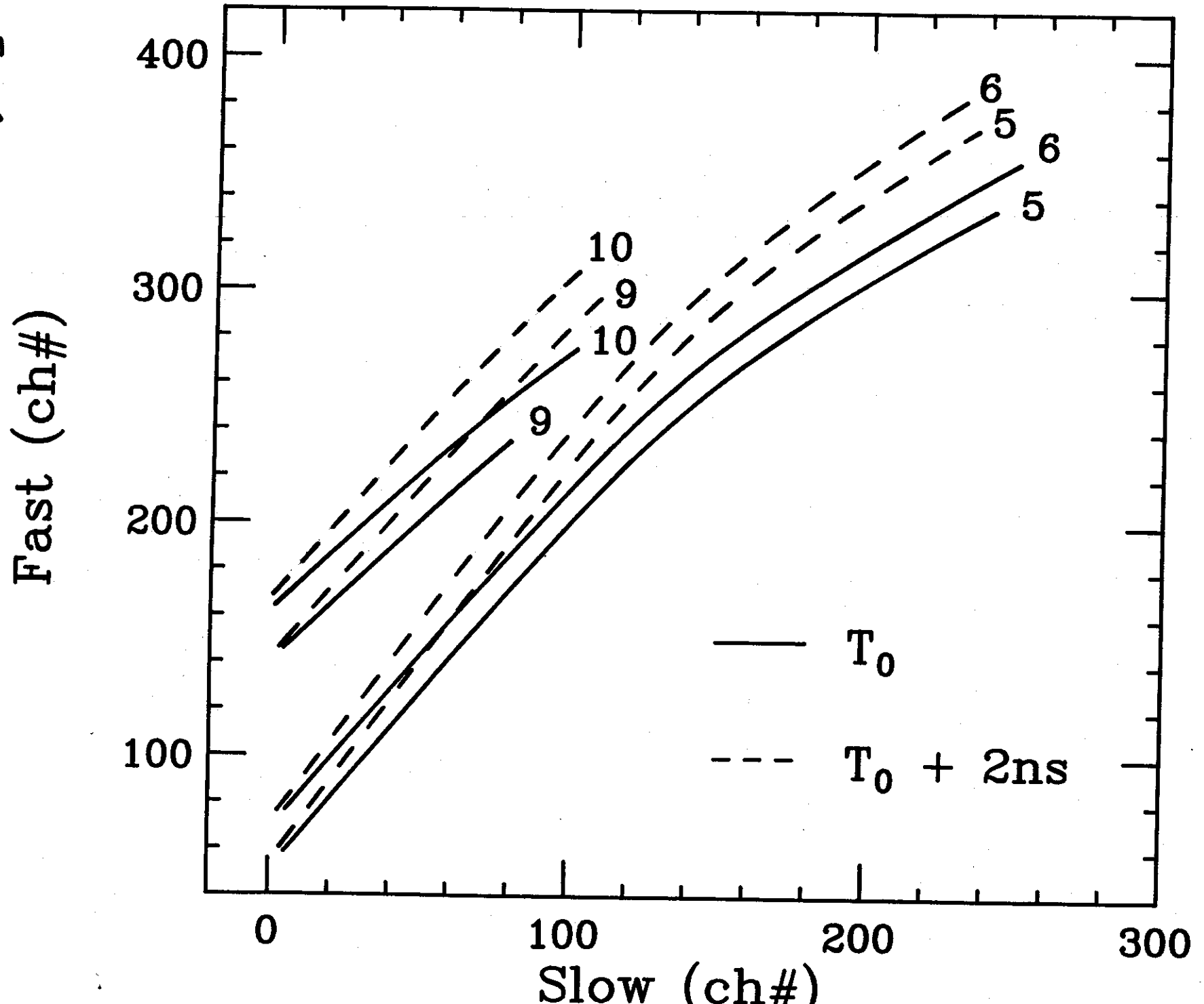
400
300
200
100
0
100
200
300
Fast (ch#)
Slow (ch#)
6
5
6
5
10
9
10
9
T_0
T_0 + 2ns

MSU-90-054

Fig. 20